

# Red-shift parametrizations of dark energy and observational constraint on their parameters: Galileon gravity as background

Prabir Rudra<sup>1</sup>

*Department of Mathematics, Asutosh College, Kolkata-700 026, India.*

Chayan Ranjit<sup>2</sup>

*Department of Mathematics, Egra S. S. B. College, Purba Medinipur-721429, W.B. India.*

Sujata Kundu<sup>3</sup>

*Department of Information Technology, Narula Institute of Technology, Kolkata-700109, India*

## Abstract

In this work, FRW universe filled with dark matter (perfect fluid with negligible pressure) along with dark energy in the background of Galileon gravity is considered. Four dark energy models with different EoS parametrizations have been employed namely, Linear, CPL, JBP and Logarithmic parametrizations. From Stern, Stern+BAO and Stern+BAO+CMB joint data analysis, we have obtained the bounds of the arbitrary parameters  $\omega_0$  and  $\omega_1$  by minimizing the  $\chi^2$  test. The best-fit values and bounds of the parameters are obtained at 66%, 90% and 99% confidence levels which are shown by closed confidence contours in the figures. For the logarithmic model unbounded confidence contours are obtained and hence the model parameters could not be finitely constrained. The distance modulus  $\mu(z)$  against redshift  $z$  has also been plotted for our predicted theoretical models for the best fit values of the parameters and compared with the observed Union2 data sample and SNe Type Ia 292 data and we have shown that our predicted theoretical models permits the observational data sets. From the data fitting it is seen that at lower redshifts ( $z < 0.3$ ) the SNe Type Ia 292 data gives a better fit with our theoretical models compared to the Union2 data sample. So, from the data analysis, SNe Type Ia 292 data is the more favoured data sample over its counterpart given the present choice of free parameters. From the study, it is also seen that the logarithmic parametrization model is less supported by the observational data. Finally we have generated the plot for the deceleration parameter against the redshift parameter for all the theoretical models and compared the results with the work of Farooq et al, 2013.

Keywords: Dark energy, Dark matter, Modified gravity, observation, data, redshift, parametrization.

*Pacs. No.: 98.80.-k, 98.80.Es, 95.35.+d, 95.36.+x*

---

<sup>1</sup>prudra.math@gmail.com

<sup>2</sup>chayanranjit@gmail.com

<sup>3</sup>sujatakundu10@gmail.com

# 1 Introduction

Over the past decade the most pressing goal for modern cosmology has been to find a proper explanation for the recent cosmic acceleration as confirmed from the observations of type Ia Supernovae and Cosmic Microwave Background (CMB) [1, 2, 3, 4, 5] radiation. The standard explanation invokes an unknown component which has the property of positive energy density and negative pressure, known as “dark energy”. Different observations have also been shown that the contributions of dark energy and dark matter are respectively about 70% and 26% of the total energy of the universe. The phenomenon of the accelerated expansion of the universe has also been strongly confirmed by some other independent experiments like Sloan Digital Sky Survey (SDSS) [6], Baryonic Acoustic Oscillation (BAO) [8], WMAP data analysis [9, 10] etc. Over the past decade, there have been many theoretical models which mimic the dark energy behaviors. The simplest of them is the cosmological constant in which the equation of state is independent of the cosmic time and which fit the observations well. This model is the so-called  $\Lambda$ CDM model, containing a mixture of cosmological constant  $\Lambda$  and cold dark matter (CDM). However, this model is plagued by two famous problems, namely “fine-tuning” and the “cosmic coincidence” problem. In order to solve these two problems, numerous dynamical dark energy models were suggested, whose equation of state evolves with cosmic time. The scalar field or quintessence [11, 12] is one of the most favourite candidate of dark energy which produce sufficient negative pressure to drive the cosmic acceleration. In order to alleviate the cosmological-constant problems and explain the accelerated expansion, many dynamical dark energy models have been proposed, such as K-essence, Tachyon, Phantom, quintom, Chaplygin gas model, etc [13, 14, 15, 16, 17]. Interaction between dark energy and dark matter have been identified as a very important tool to address these problems. As a result interacting dark energy models including Modified Chaplygin gas [18], holographic dark energy model [19] and braneworld model [20] have been proposed. Since the discovery of General theory of relativity, the most pressing objective for cosmology has been found as the complete theory of quantum gravity i.e., the theory of everything. Relentless efforts and their results can be found widely in literature. Recently, such efforts using the principle of quantum gravity, led to the proposals of agegraphic dark energy (ADE) and the new agegraphic dark energy (NADE) models by Cai [21] and Wei et al. [22] respectively. Many theoretical models have been tallied with the observations using different data sets, say TONRY, Gold sample data sets [23, 3, 24, 25] etc. In Einstein’s gravity, the modified Chaplygin gas [18] best fits with the 3 year WMAP and the SDSS data with the choice of parameters  $A = 0.085$  and  $\alpha = 1.724$  [26] which are improvements over the previous ones  $-0.35 < A < 0.025$  [27].

Another possibility of the accelerated expansion is attributed to the fact that general relativity is only accurate on small scales and therefore needs modification on cosmological distances. This led to the proposal of modified gravity theories. In this case, cosmic acceleration would arise not to from dark energy as a constituent substance but rather from the dynamics of modified gravity. Modified gravity constitutes an interesting dynamical alternative to  $\Lambda$ CDM cosmology regarding given the fact that it is also able to describe the current acceleration in the expansion of our universe. One of the simplest modified gravity is DGP brane-world model [28]. The other alternative approach dealing with the acceleration problem of the Universe is changing the gravity law through the modification of action of gravity by means of using  $f(R)$  gravity [29, 30] instead of the Einstein-Hilbert action. Some of these models, such as  $1/R$  and logarithmic models, produced an accelerated expansion for the Universe at the present time [31]. Other modified gravity includes  $f(T)$  gravity,  $f(G)$  gravity, Gauss-Bonnet gravity, Horava-Lifshitz gravity, Brans-Dicke gravity, etc [32, 33, 34, 35, 36].

Of late an infrared modification of classical gravitation was proposed, which is a generalization of the 4D effective theory in the DGP model [37]. The theory considers a self-interaction term of the form  $\Box \phi (\nabla \phi)^2$  in order to recover GR in high density regimes. The most notable feature of the theory is that it is invariant under the Galileon shift symmetry  $\delta_\mu \phi \rightarrow \delta_\mu \phi + c_\mu$  in the Minkowski background. Because of this invariance, the equation of motion remains a second order differential equation, preventing the introduction of extra degrees of freedom, which are usually associated with instabilities. So we assume the FRW universe in Galileon gravity model filled with the dark matter and dark energy.

As stated earlier, in order to explain the evolution of the universe, various dark energy models have been proposed. All these models must be constrained by astronomical observations in order to bring about a consistency between the proposed theoretical models and the observational data. For any dark energy model, the Equation of state (EoS) parameter  $\omega$  plays a vital role and can reveal the nature of the model which is responsible for the cosmic acceleration. Different form of EoS lead to different dynamical nature and may influence the evolution of the Universe considerably. The EoS parameter  $\omega$  and its time derivative with respect to Hubble time are

currently constrained by the distance measurements of the type Ia supernova. From literature it is seen that the current observational data constrain the range of EoS as  $-1.38 < \omega < -0.82$  [38]. Recently, the combination of WMAP3 and Supernova Legacy Survey data showed a significant constraint on the EOS  $\omega = -0.97^{+0.07}_{-0.09}$  for the dark energy in a flat universe [39]. Recently, some parametrizations for the variation of EOS parameters  $\omega(z)$  have been proposed describing the DE component. We will discuss them in detail in section 3.

It is a known fact that the standard big bang model of cosmology is crippled by various problems such as the horizon problem, the flatness problem, the singularity problem, etc. Considering the inflationary model, we have been able to explain the flatness problem. Now for a flat universe filled with matter and dark energy, an accurate knowledge of  $\Omega_{de}$  and  $\omega_{de}$  for dark energy can only be obtained if we have a proper knowledge of  $\Omega_m$  for dark matter and  $H(z)$  [23, 40]. For  $z > 0.01$ , we see that the TONRY data with 230 data points [24] with 23 data points from Barris et al. [25] is quite acceptable. In the redshift range  $1 < z < 1.6$ , the GOLD sample of Riess et al. [3] with 156 data points is valid. From the CMBR data one finds that  $\Omega_\Lambda + \Omega_m = 1$  [10]. From the most recently obtained Riess data set the best fit value of  $\Omega_m$  is obtained as  $0.31 \pm 0.04$ . This value matches with the value of  $\Omega_m = 0.29^{+0.05}_{-0.03}$  obtained from the previous Riess data [2]. In Chowdhury et al. [23] the value was found to be  $0.31 \pm 0.08$ . For a flat universe, the best fit value for the equation of state parameter  $w$  for union 2 data sample is  $\omega = -0.997^{+0.050}_{-0.054}(\text{stat})^{+0.077}_{-0.082}(\text{stat+sys together})$ . For a curved one, the value is  $\omega = -1.038^{+0.056}_{-0.059}(\text{stat})^{+0.093}_{-0.097}(\text{stat+sys together})$  [41].

The success of any dark energy or modified gravity model, depends basically on its consistency with the observational data. This is our basic motivation for the work. We reconstruct the hubble parameter  $H$  using the parameters of dark energy, dark matter and modified gravity. Then we set up a comparison scenario between the reconstructed  $H$  ( $H_{theoretical}$ ) and the values of  $H$  obtained from observational data ( $H_{observational}$ ). This is accomplished by the procedure of chi-square test. Recently, numerous works can have appeared in the literature, which aims at constraining dark energy model parameters using Stern and union2 data sets [42, 43, 44, 45, 46]. The basic concepts of Galileon gravity theory are presented in section 2. The behaviour of some reconstructed cosmological parameters is studied in section 3. Some basic calculations using the Galileon gravity and parametrized dark energy models is given in section 4. The observational data analysis tools in observed Hubble data (OHD) or  $H(z)$ - $z$  (Stern), OHD+BAO and OHD+BAO+CMB for  $\chi^2$  minimum test will be studied in section 5 and we will also investigate the bounds of unknown parameters ( $\omega_0, \omega_1$ ) for the various dark energy parametrizations by fixing other parameters. The best-fit values of the parameters are obtained at 66%, 90% and 99% confidence levels. The redshift magnitude observations for our theoretical parametrization models in Galileon gravity for the best fit values of the parameters and the observed SNe Ia union2 data sample is studied in section 6. Analysis of our theoretical models with SNe Type Ia 292 data is given in section 7. Finally the paper ends with a discussion in section 8.

## 2 Basic equations of Galileon gravity

The Galileon gravity theory is described by the action [37, 47, 48, 49, 50]:

$$S = \int d^4x \sqrt{-g} \left[ \phi R - \frac{w}{\phi} (\nabla \phi)^2 + f(\phi) \square \phi (\nabla \phi)^2 + \mathcal{L}_m \right] \quad (1)$$

where  $\phi$  is the Galileon field,  $w$  is known as Brans-Dicke (BD) parameter, the coupling function  $f(\phi)$  has dimension of length,  $(\nabla \phi)^2 = g^{\mu\nu} \nabla_\mu \phi \nabla_\nu \phi$ ,  $\square \phi = g^{\mu\nu} \nabla_\mu \nabla_\nu \phi$  and  $\mathcal{L}_m$  is the matter Lagrangian. Variation of Eqn. (1) with respect to the metric  $g_{\mu\nu}$  gives the Einstein's equations,

$$G_{\mu\nu} = \frac{T_{\mu\nu}}{2\phi} + \frac{1}{\phi} (\nabla_\mu \nabla_\nu \phi - g_{\mu\nu} \square \phi) + \frac{w}{\phi^2} \left[ \nabla_\mu \phi \nabla_\nu \phi - \frac{1}{2} g_{\mu\nu} (\nabla \phi)^2 \right] - \frac{1}{\phi} \left\{ \frac{1}{2} g_{\mu\nu} \nabla_\lambda [f(\phi) (\nabla \phi)^2] \nabla^\lambda \phi - \nabla_\mu [f(\phi) (\nabla \phi)^2] \nabla_\nu \phi + f(\phi) \nabla_\mu \phi \nabla_\nu \phi \square \phi \right\} \quad (2)$$

For the Friedmann-Robertson-Walker background metric, the Einstein's field eqns for Galileon gravity gives,

$$3H^2 = \frac{\rho}{2\phi} - 3HI + \frac{w}{2} I^2 + \phi^2 f(\phi) \left( 3H - \frac{\alpha_1}{2} I \right) I^3 \quad (3)$$

and

$$-3H^2 - 2\dot{H} = \frac{p}{2\phi} + \dot{I} + I^2 + 2HI + \frac{w}{2}I^2 - \phi^2 f(\phi) \left( \dot{I} + \frac{2+\alpha_1}{2}I^2 \right) I^2 \quad (4)$$

where  $H(t) = \frac{\dot{a}}{a}$ ,  $I(t) = \frac{\dot{\phi}}{\phi}$  and  $\alpha_n[\phi(t)] = \frac{d^n \ln f}{d \ln \phi^n}$ .

Here  $\rho = \rho_{de} + \rho_m$  and  $p = p_{de} + p_m$ , where  $\rho_m, p_m$  are the energy density and pressure of the dark matter and  $\rho_{de}, p_{de}$  are respectively the energy density and pressure contribution of some dark energy.

### 3 Some parametrizations on EoS parameter

Recently some parametrizations for the variation of EOS parameters  $\omega(z)$  have been proposed describing the DE component. Here we discuss some of them.

#### 3.1 Linear Parametrization

Here the EoS is given by [51]

$$\omega(z) = \omega_0 + \omega_1 z \quad (5)$$

Here  $\omega_0 = -1/3$  and  $\omega_1 = -0.9$  with  $z < 1$  when Einstein gravity has been considered. This grows increasingly unsuitable for  $z > 1$ .

#### 3.2 Chevallier-Polarski-Lindler (CPL) Parametrization

Here the EoS is given by

$$\omega(z) = \omega_0 + \omega_1 \frac{z}{1+z} \quad (6)$$

This ansatz was first discussed by Chevallier and Polarski [52] and later studied more elaborately by Linder [53]. In Einstein gravity the best fit values for this model while fitting with SN1a gold data set are  $\omega_0 = -1.58$  and  $\omega_1 = 3.29$ . This parametrization has several advantages over its predecessor. Some of them are: 1) It has a manageable 2-dimensional phase space; 2) reduces to the old linear redshift behaviour at low redshift; 3) has a well behaved and bounded behaviour for high redshift; 4) highly accurate in reconstructing many scalar field equations of state and the resulting distance-redshift relations; 5) highly sensitive to observational data and 6) simple physical interpretation. In addition to the above advantages, the new parametrization is also more accurate than the previous one. The most remarkable thing about the parametrization is that, it reconstructs the distance-redshift behaviour of the SUGRA model [54] to 0.2% over the entire range out to the last scattering surface ( $z \approx 1100$ ).

#### 3.3 Jassal-Bagla-Padmanabhan (JBP) Parametrization

Here the EoS is given by [55]

$$\omega(z) = \omega_0 + \omega_1 \frac{z}{(1+z)^2} \quad (7)$$

A fairly rapid evolution of this EoS is allowed so that  $\omega(z) \geq -1/2$  at  $z > 0.5$  is consistent with the supernovae observation in Einstein gravity. From the EoS it can be seen that  $\omega(0) = \omega_0$  and  $\omega(\infty) = \omega_0$ . For a standard cosmological model with a hot big bang to be valid, we must have  $\omega(z \gg 1) \leq -1/3$ .

#### 3.4 Logarithmic Parametrization

Here the EoS is given by [56, 57]

$$\omega(z) = \omega_0 + \omega_1 \log(1+z) \quad (8)$$

This model is sparsely found in literature, and therefore very little is known about the behaviour of this model. It has been used now and then for parametrization of dark energy. Here we will analyze it and try to compare it with other models. This will help us to understand its importance in cosmology and also to find out the reason why it has been so seldom studied in past. This is the basic reason for the inclusion of this model in the present study.

## 4 Basic calculations on Galileon gravity using various EoS parametrizations

Here we will consider the flat, homogeneous and isotropic universe described by the FRW background metric. The corresponding Einstein equations in Galileon gravity are given by eqns.(3) and (4). The DE equation of state is taken as  $p_{de} = \omega(z)\rho_{de}$ . We neglect the pressure contribution of matter, i.e.  $p_m = 0$ . The independent conservation equations for DE and DM are given as,

$$\dot{\rho}_{de} + 3H(\rho_{de} + p_{de}) = 0 \quad (9)$$

and

$$\dot{\rho}_m + 3H\rho_m = 0 \quad (10)$$

From eqn.(10), we have

$$\rho_m = \rho_{m0} (1+z)^3 \quad (11)$$

where we have used the relation  $a = \frac{1}{1+z}$ ,  $z$  being the cosmological redshift parameter. Here  $\rho_{m0}$  is a constant. Integrating equation (9) for the four DE models we get four different solutions for DE density. Now, we consider dimensionless density parameters  $\Omega_{m0} = \frac{\rho_{m0}}{3H_0^2}$  and  $\Omega_{de0} = \frac{\rho_{de0}}{3H_0^2}$  and for simplicity choosing  $f(\phi) = f_0\phi^n$  and  $\phi = \phi_0 a^m$  ( $f_0 > 0$ ,  $\phi_0 > 0$ ,  $m > 0$ ,  $n > 0$ ) in the power law form, [43] we have the expression for Hubble parameter  $H$  in terms of redshift parameter  $z$  as follows (from eq. 3):

$$H(z) = \frac{1}{2(6f_0m^3\phi_0^{3+n} - f_0m^4n\phi_0^{3+n})} \left[ -(m^2w - 6m - 6)(1+z)^{m(2+n)}\phi_0 \right. \\ \left. + \left\{ \left( (m^2w - 6m - 6)(1+z)^{m(2+n)}\phi_0 \right)^2 - f_0m^4n\phi_0^{3+n} - 12H_0^2 \left( (1+z)^{3+m(3+n)}\Omega_{m0} + \right. \right. \right. \\ \left. \left. \left. (1+z)^{m(3+n)} \frac{\rho_{de}}{3H_0^2} \right) 6f_0m^3\phi_0^{3+n} \right\}^{\frac{1}{2}} \right] \quad (12)$$

### 4.1 Expressions for Linear parametrization

Using equation (5), we integrate equation (9) and get the expression for DE density as

$$\rho_{de} = \rho_{de0} (1+z)^{3(1+\omega_0-\omega_1)} \exp\{3\omega_1(1+z)\} \quad (13)$$

where  $\rho_{de0}$  is a constant. In terms of the above mention dimensionless density parameters and redshift parameter ( $z$ ) we calculate the Hubble parameter as follows,

$$H_{lin}(z) = \left[ \frac{3(1+z)^{m(2+n)+3\omega_1}\phi_0(1+m-\frac{1}{3}m^2w)}{f_0m^3\phi_0^{3+n}(1+z)^{3\omega_1}(6-mn)} + \left( \left( \left( 36(1+z)^{2m(2+n)+6\omega_1}\phi_0^2 \left( 1+m^2-\frac{1}{6}m^2w \right)^2 \right) \right. \right. \right. \\ \left. \left. \left. + 12H_0^2 \left( (1+z)^{m+m(2+n)+3\omega_1}\Omega_{m0}(1+3z+3z^2+z^3) + \exp\{3\omega_1(1+z)\}(1+z)^{m+m(2+n)+3\omega_0}\Omega_{de0} \right. \right. \right. \right. \\ \left. \left. \left. (1+3z+3z^2+z^3) f_0m^3(1+z)^{3\omega_1}\phi_0^{3+n}(mn-6) \right)^{1/2} \right) \times \frac{1}{2f_0m^3(1+z)^{3\omega_1}\phi_0^{3+n}(mn-6)} \right]^{1/2} \quad (14)$$

## 4.2 Expressions for CPL parametrization

For this DE parametrization the DE density is obtained as,

$$\rho_{de} = \rho_{de0} (1+z)^{3(1+\omega_0+\omega_1)} \exp\{3\omega_1 (1+z)\} \quad (15)$$

Using the dimensionless density parameters, the expression for the Hubble parameter in terms of the redshift is obtained as,

$$\begin{aligned} H_{CPL}(z) = & \left[ \frac{3(1+z)^{m(2+n)} \phi_0 (1+m-\frac{1}{6}m^2w)}{f_0 m^3 \phi_0^{3+n} (6-mn)} + \frac{1}{2f_0 m^3 \phi_0^{3+n} (6-mn)} \left( \left( \left( 36(1+z)^{2m(2+n)} \phi_0^2 \left( 1+m-\frac{1}{6}m^2w \right)^2 \right) \right. \right. \right. \\ & + 12H_0^2 \left( (1+z)^{m+m(2+n)} \Omega_{m0} (1+3z+3z^2+z^3) + \exp\left\{ \frac{3\omega_1}{(1+z)} \right\} (1+z)^{m+m(2+n)+3\omega_0+3\omega_1} \Omega_{de0} \right. \\ & \left. \left. \left. (1+3z+3z^2+z^3) \right) f_0 m^3 (1+z)^{3\omega_1} \phi_0^{3+n} (mn-6) \right)^{1/2} \times \frac{1}{2f_0 m^3 \phi_0^{3+n} (mn-6)} \right]^{1/2} \end{aligned} \quad (16)$$

## 4.3 Expressions for JBP parametrization

Here the DE density is obtained as,

$$\rho_{de} = \rho_{de0} (1+z)^{3(1+\omega_0)} \exp\left\{ -\frac{3\omega_1 (z+\frac{1}{2})}{(1+z)^2} \right\} \quad (17)$$

Using the dimensionless density parameters, the expression for the Hubble parameter in terms of the redshift is obtained as,

$$\begin{aligned} H_{JBP}(z) = & \frac{1}{\sqrt{2}} \left[ \left( \frac{1}{f_0 m^3 (-6+mn)} \exp\left\{ -\frac{3(\omega_1+2z\omega_1)}{2(1+z)^2} \right\} \phi_0^{-3-n} \left( \exp\left\{ \frac{3(\omega_1+2z\omega_1)}{2(1+z)^2} \right\} (-6+m(-6+mw)) \right. \right. \right. \\ & (1+z)^{m(2+n)} \phi_0 \left( \exp\left\{ \frac{3(\omega_1+2z\omega_1)}{(1+z)^2} \right\} (6+m(6-mw))^2 (1+z)^{2m(2+n)} \phi_0^2 + 12e^{\frac{3(\omega_1+2z\omega_1)}{2(1+z)^2}} f_0 H_0^2 m^3 (-6+mn) \right. \\ & \left. \left. \left. (1+z)^{3+m(3+n)} \phi_0^{3+n} \left( \exp\left\{ \frac{3(\omega_1+2z\omega_1)}{2(1+z)^2} \right\} \Omega_{m0} + (1+z)^{3\omega_0} \Omega_{x0} \right) \right)^{1/2} \right) \right)^{1/2} \right] \end{aligned} \quad (18)$$

## 4.4 Expressions for Logarithmic parametrization

For this parametrization model, the DE density is obtained as,

$$\rho_{de} = \rho_{de0} (1+z)^{3(1+\omega_0+\omega_1)} \quad (19)$$

Using the dimensionless density parameters, the expression for the Hubble parameter in terms of the redshift is obtained as,

$$\begin{aligned} H_{Log}(z) = & \left[ \left( \frac{1}{2f_0 m^3 (-6+mn)} \phi_0^{-3-n} \left( -6(1+z)^{m(2+n)} \phi_0 - 6m(1+z)^{m(2+n)} \phi_0 + m^2w (1+z)^{m(2+n)} \phi_0 + ((6+6m \right. \right. \right. \\ & \left. \left. \left. -m^2w)^2 (1+z)^{2m(2+n)} \phi_0^2 + 12f_0 H_0^2 m^3 (-6+mn) (1+z)^{3+m(3+n)} \phi_0^{3+n} \left( \Omega_{m0} + (1+z)^{3(\omega_0+\omega_1)} \Omega_{de0} \right) \right)^{1/2} \right) \right]^{1/2} \end{aligned} \quad (20)$$

## 5 Observational data analysis mechanism

In the following subsections, we present the observational data analysis mechanism for Stern, Stern+BAO and Stern+BAO+CMB observations. We use the  $\chi^2$  minimum test from theoretical Hubble parameter with the observed data set and find the best fit values of unknown parameters for different confidence levels. From the above expressions, we see that  $H(z)$  contains the unknown parameters like  $\omega_0$ ,  $\omega_1$ ,  $\Omega_{m0}$ ,  $\Omega_{de0}$ ,  $w$ ,  $n$ ,  $m$ ,  $f_0$ ,  $\phi_0$ . Now the relation between two parameters will be obtained by fixing the other parameters and by using observational data set. Eventually the bounds of the parameters will be obtained by using this observational data analysis mechanism.

$z$	$H(z)$	$\sigma(z)$
0	73	$\pm 8$
0.1	69	$\pm 12$
0.17	83	$\pm 8$
0.27	77	$\pm 14$
0.4	95	$\pm 17.4$
0.48	90	$\pm 60$
0.88	97	$\pm 40.4$
0.9	117	$\pm 23$
1.3	168	$\pm 17.4$
1.43	177	$\pm 18.2$
1.53	140	$\pm 14$
1.75	202	$\pm 40.4$

**Table 1:** The Hubble parameter  $H(z)$  and the standard error  $\sigma(z)$  for different values of redshift  $z$ .

### 5.1 Analysis with Stern data

We analyze the model, using observed value of Hubble parameter at different redshifts (twelve data points) listed in observed Hubble data by Stern et al. [58]. The Hubble parameter  $H(z)$  and the standard error  $\sigma(z)$  for different values of redshift  $z$  are given in Table 1. Since we are using testing of hypothesis, so before proceeding, we form our null and alternate hypothesis which are given below.

**Null Hypothesis:**  $H_0: H_{theoretical} = H_{observational}$

**Alternative Hypothesis:**  $H_1: H_{theoretical} \neq H_{observational}$

Here we test the null hypothesis  $H_0$  against the alternative hypothesis  $H_1$ . For this purpose we first form the  $\chi^2$  statistics as a sum of standard normal distribution as follows:

$$\chi_{Stern}^2 = \sum \frac{(H(z) - H_{obs}(z))^2}{\sigma^2(z)} \quad (21)$$

where  $H(z)$  and  $H_{obs}(z)$  are theoretical and observational values of Hubble parameter at different redshifts respectively. Here,  $H_{obs}$  is a nuisance parameter and can be safely marginalized. We consider the present value of Hubble parameter  $H_0 = 72 \pm 8 \text{ Kms}^{-1} \text{ Mpc}^{-1}$  and a fixed prior distribution. Here we shall determine best fit value of the parameters  $(\omega_1, \omega_0)$  by minimizing the above distribution  $\chi_{Stern}^2$  and fixing the other unknown parameters with the help of Stern data.

We now plot the graph for different confidence levels. Now our best fit analysis with Stern observational data support the theoretical range of the parameters. The 66% (solid, blue), 90% (dashed, red) and 99% (dashed, black) contours are plotted in figures 1a, 1b, 1c and 1d for  $\Omega_{m0} = 0.28$ ,  $\Omega_{de0} = 0.72$ ,  $n = 3.155$ ,  $m = 2$ ,  $\omega = -25$ ,  $f_0 = 0.9$ ,  $\phi_0 = 0.1$ . The best fit values of  $(\omega_1, \omega_0)$  are tabulated in Table 2. Here the values of  $\Omega_{m0}$  and  $\Omega_{de0}$  are motivated from the recent cosmological observational data. The value of  $\omega$  is chosen in accordance with reference [7]. The rest of the parameters namely,  $f_0$ ,  $\phi_0$ ,  $m$  and  $n$  arises due to our particular choice function of the scalar field. Due to their secondary importance we consider them as free parameters and their values are fine tuned in such a way so that effective closed contours are obtained.

## 5.2 Joint analysis with Stern+BAO datasets

The method of joint analysis, the Baryon Acoustic Oscillation (BAO) peak parameter value has been proposed by [8] and we shall use their approach. Sloan Digital Sky Survey (SDSS) survey is one of the first redshift survey by which the BAO signal has been directly detected at a scale  $\sim 100$  Mpc. The said analysis is actually the combination of angular diameter distance and Hubble parameter at that redshift. This analysis is independent of the measurement of  $H_0$  and not containing any particular dark energy. Here we examine the parameters  $\omega_1$  and  $\omega_0$  for parametrized DE model from the measurements of the BAO peak for low redshift (with range  $0 < z < 0.35$ ) using standard  $\chi^2$  analysis. The error is corresponding to the standard deviation, where we consider Gaussian distribution. Low-redshift distance measurements is lightly dependent on different cosmological parameters, the equation of state of dark energy and have the ability to measure the Hubble constant  $H_0$  directly. The BAO peak parameter may be defined by

$$\mathcal{A} = \frac{\sqrt{\Omega_m}}{E(z_1)^{1/3}} \left( \frac{1}{z_1} \int_0^{z_1} \frac{dz}{E(z)} \right)^{2/3} \quad (22)$$

Here  $E(z) = H(z)/H_0$  is the normalized Hubble parameter, the redshift  $z_1 = 0.35$  is the typical redshift of the SDSS sample and the integration term is the dimensionless comoving distance to the redshift  $z_1$ . The value of the parameter  $\mathcal{A}$  for the flat model of the universe is given by  $\mathcal{A} = 0.469 \pm 0.017$  using SDSS data [8] from luminous red galaxies survey. Now the  $\chi^2$  function for the BAO measurement can be written as

$$\chi_{BAO}^2 = \frac{(\mathcal{A} - 0.469)^2}{(0.017)^2} \quad (23)$$

Now the total joint data analysis (Stern+BAO) for the  $\chi^2$  function may be defined by

$$\chi_{total}^2 = \chi_{Stern}^2 + \chi_{BAO}^2 \quad (24)$$

According to our analysis the joint scheme(Stern+BAO) gives the best fit values of  $(\omega_1, \omega_0)$  in Table 3. Finally we draw the contours for the 66% (solid, blue), 90% (dashed, red) and 99%(dashed, black) confidence limits depicted in figures 2a, 2b, 2c and 2d for  $\Omega_{m0} = 0.28$ ,  $\Omega_{de0} = 0.72$ ,  $\alpha = 0.001$ ,  $n = 0.5, m = 10$ ,  $\omega = -3$ ,  $w_m = 0.03$ ,  $f_0 = 0.01$ ,  $\phi_0 = 0.01$ .

## 5.3 Joint analysis with Stern+BAO+CMB datasets

One interesting geometrical probe of dark energy can be determined by the angular scale of the first acoustic peak through angular scale of the sound horizon at the surface of last scattering which is encoded in the CMB power spectrum Cosmic Microwave Background (CMB) shift parameter is defined by [59, 60, 61]. It is not sensitive with respect to perturbations but are suitable to constrain model parameter. The CMB power spectrum first peak is the shift parameter which is given by

$$\mathcal{R} = \sqrt{\Omega_m} \int_0^{z_2} \frac{dz}{E(z)} \quad (25)$$

where  $z_2$  is the value of redshift at the last scattering surface. From WMAP7 data of the work of Komatsu et al. [62] the value of the parameter has obtained as  $\mathcal{R} = 1.726 \pm 0.018$  at the redshift  $z = 1091.3$ . Now the  $\chi^2$  function for the CMB measurement can be written as

$$\chi_{CMB}^2 = \frac{(\mathcal{R} - 1.726)^2}{(0.018)^2} \quad (26)$$

Now when we consider three cosmological tests together, the total joint data analysis (Stern+BAO+CMB) for the  $\chi^2$  function may be defined by

$$\chi_{TOTAL}^2 = \chi_{Stern}^2 + \chi_{BAO}^2 + \chi_{CMB}^2 \quad (27)$$

Now the best fit values of  $(\omega_1, \omega_0)$  for joint analysis of BAO and CMB with Stern observational data support the theoretical range of the parameters given in Table 4. The 66% (solid, blue), 90% (dashed, red) and 99% (dashed, black) contours are plotted in figures 3a, 3b, 3c and 3d for  $\Omega_{m0} = 0.28$ ,  $\Omega_{de0} = 0.72$ ,  $\alpha = 0.001$ ,  $n = 0.5, m = 10$ ,  $\omega = -3$ ,  $w_m = 0.03$ ,  $f_0 = 0.01$ ,  $\phi_0 = 0.01$ .



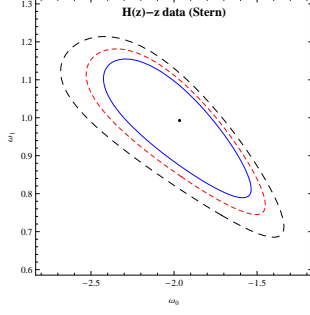


Fig.1a

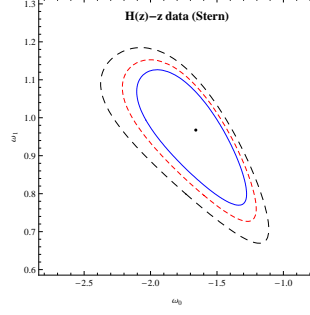


Fig.1b

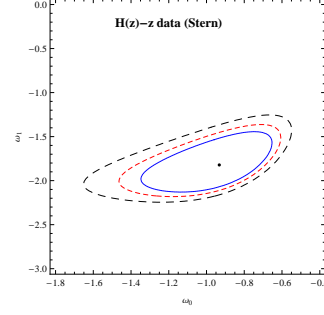


Fig.1c

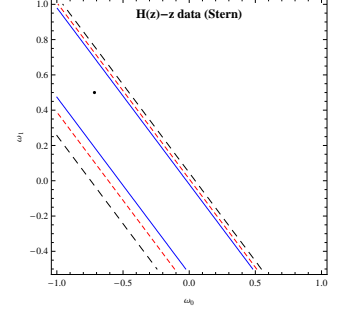


Fig.1d

**Figs 1a, 1b, 1c and 1d** show the variation of  $\omega_0$  with  $\omega_1$  for different confidence levels for linear, CPL, JBP and logarithmic models respectively. The 66% (solid, blue, the innermost contour), 90% (dashed, red, next to the innermost contour), and 99% (dashed, black, the outermost contour) contours are plotted in these figures for the  $H(z) - z$  (Stern) analysis.

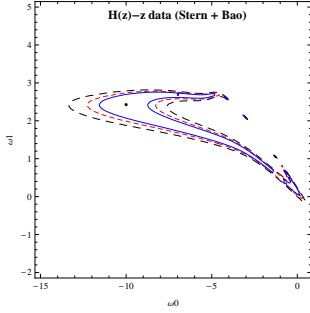


Fig.2a

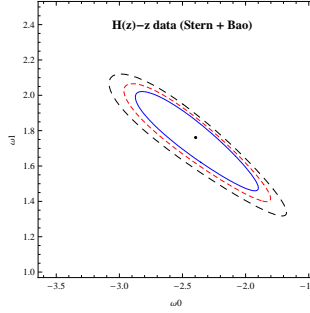


Fig.2b

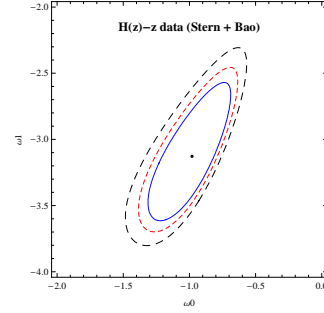


Fig.2c

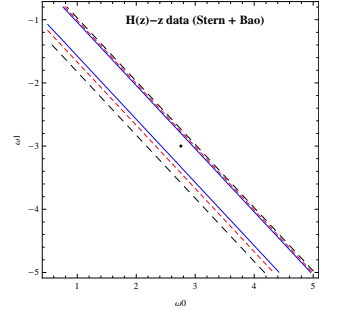


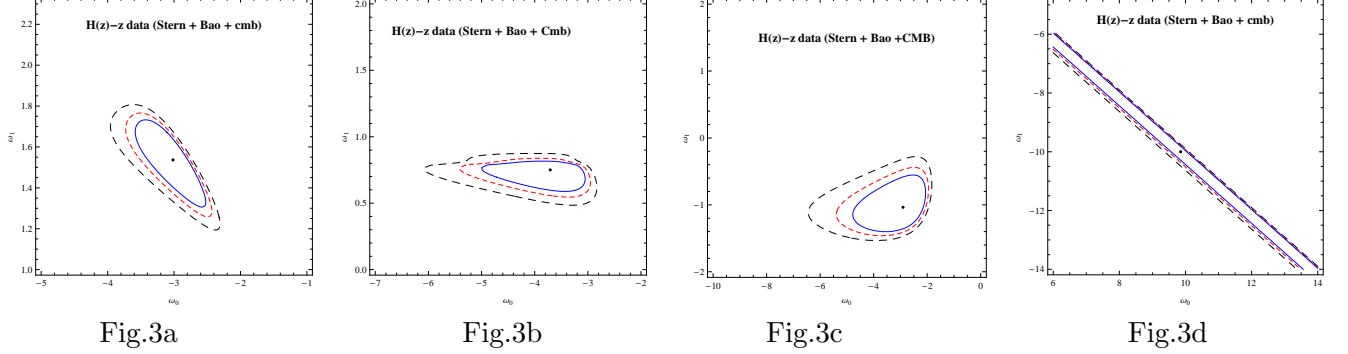
Fig.2d

**Figs 2a, 2b, 2c and 2d** show the variation of  $\omega_0$  with  $\omega_1$  for different confidence levels for linear, CPL, JBP and logarithmic models respectively. The 66% (solid, blue, the innermost contour), 90% (dashed, red, next to the innermost contour), and 99% (dashed, black, the outermost contour) contours are plotted in these figures for the  $H(z)z$  (Stern+Bao) joint analysis.

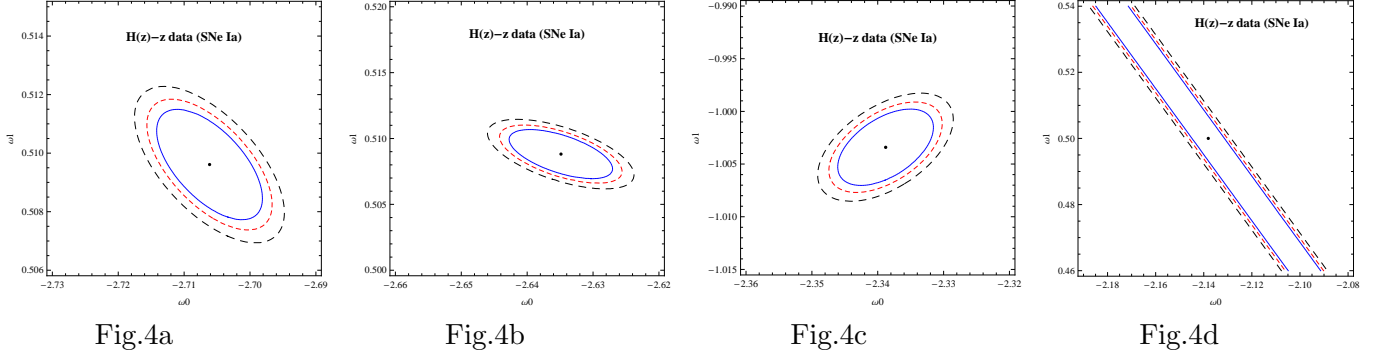
DE models	Best fit values		
	$\omega_0$	$\omega_1$	$\chi^2_{min}$
Linear	-1.96664	0.992802	11.4933
CPL	-1.65925	0.967584	8.4682
JBP	-0.932444	-1.82202	7.88769
Log	-0.716018	0.5	127.572

**Table 2:** STERN: The best fit values of  $\omega_0$  and  $\omega_1$  and the minimum values of  $\chi^2$  for different redshift parametrization models.

DE models	Best fit values		
	$\omega_0$	$\omega_1$	$\chi^2_{min}$
Linear	-10	2.42671	928.664
CPL	-2.39571	1.76133	773.265
JBP	-0.980504	-3.12768	781.012
Log	2.75676	-3	903.023



**Figs 3a, 3b, 3c and 3d** show the variation of  $\omega_0$  with  $\omega_1$  for different confidence levels for linear, CPL, JBP and logarithmic models respectively. The 66% (solid, blue, the innermost contour), 90% (dashed, red, next to the innermost contour), and 99% (dashed, black, the outermost contour) contours are plotted in these figures for the  $H(z)z$  (Stern+BAO+CMB) joint analysis.



**Figs 4a, 4b, 4c and 4d** show the variation of  $\omega_0$  with  $\omega_1$  for different confidence levels for linear, CPL, JBP and logarithmic models respectively. The 66% (solid, blue, the innermost contour), 90% (dashed, red, next to the innermost contour), and 99% (dashed, black, the outermost contour) contours are plotted in these figures for the  $H(z)z$  of SNe Type Ia 292 data.

**Table 3:** STERN+BAO: The best fit values of  $\omega_0$  and  $\omega_1$  and the minimum values of  $\chi^2$  for different redshift parametrization models.

<i>DE models</i>	<i>Best fit values</i>		
	$\omega_0$	$\omega_1$	$\chi^2_{min}$
<i>Linear</i>	-3.01522	1.53659	9969.52
<i>CPL</i>	-3.70734	0.750595	11645.9
<i>JBP</i>	-2.9022	-1.03615	10400.9
<i>Log</i>	9.85277	-10	10105.5

**Table 4:** STERN+BAO+CMB: The best fit values of  $\omega_0$  and  $\omega_1$  and the minimum values of  $\chi^2$  for different redshift parametrization models.

<i>DE models</i>	<i>Best fit values</i>		
	$\omega_0$	$\omega_1$	$\chi^2_{min}$
<i>Linear</i>	-2.70613	0.509612	879522.25
<i>CPL</i>	-2.63487	0.508819	867545.51
<i>JBP</i>	-2.3388	-1.00341	847931.41
<i>Log</i>	-2.13811	0.5	$1.32293 \times 10^6$

**Table 5:**  $H(z)$ -z SNe Type Ia 292: The best fit values of  $\omega_0$  and  $\omega_1$  and the minimum values of  $\chi^2$  for different redshift parametrization models.

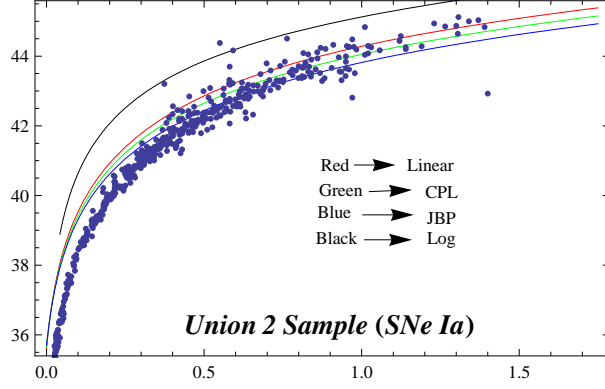


Fig.5a

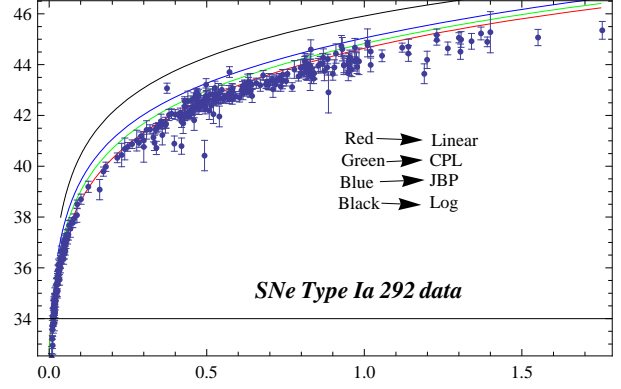


Fig.5b

**Figs 5a and 5b** show the variation of  $\mu(z)$  vs  $z$  for linear, CPL, JBP and logarithmic parametrizations (solid lines) and their comparison with observational data (blue dots). The dots denote the Union2 sample data in fig 5a and the SNe Type Ia 292 data in fig 5b.

## 6 Redshift-magnitude observations from supernovae type Ia Union2 sample (from Amanullah et al. 2010)

The Supernova Type Ia experiments provided the main evidence for the existence of dark energy. Since 1995, two teams of High- $z$  Supernova Search and the Supernova Cosmology Project have discovered several type Ia supernovas at the high redshifts [1, 2, 3, 63]. The observations directly measure the distance modulus of a Supernovae and its redshift  $z$  [64, 65]. Now, take recent observational data, including SNe Ia which consists of 557 data points and belongs to the Union2 sample [41]. From the observations, the luminosity distance  $d_L(z)$  determines the dark energy density and is defined by

$$d_L(z) = (1+z)H_0 \int_0^z \frac{dz'}{H(z')} \quad (28)$$

and the distance modulus (distance between absolute and apparent luminosity of a distance object) for Supernovas is given by

$$\mu(z) = 5 \log_{10} \left[ \frac{d_L(z)/H_0}{1 \text{ Mpc}} \right] + 25 \quad (29)$$

The best fit of distance modulus as a function  $\mu(z)$  of redshift  $z$  for our theoretical models and the Supernova Type Ia Union2 sample are drawn in figure 5a for our best fit values of  $\omega_1$  and  $\omega_0$  for (Stern) + BAO + CMB joint analysis as  $\Omega_{m0} = 0.28$ ,  $\Omega_{de0} = 0.72$ ,  $\alpha = 0.001$ ,  $n = 0.5$ ,  $m = 10$ ,  $\omega = -3$ ,  $w_m = 0.03$ ,  $f_0 = 0.01$ ,  $\phi_0 = 0.01$ . Similarly the best fit trajectories for our theoretical models are obtained and compared with SNe Type Ia 292 data in fig.5b. From the curves, we see that the theoretical parametrized DE models in Galileon gravity is in agreement with the union2 sample data and the SNe Type Ia 292 data.

## 7 Analysis with Supernovae Type Ia 292 data (from Riess et al.(2004, 2007) and Astier et al.(2006))

Here we have analyzed our theoretical parametrized DE models in the light of the Supernovae Type Ia 292 data [3, 64, 66]. The compiled data can be found in ref [67]. Bounds for the model parameters  $(\omega_0, \omega_1)$  have been obtained by constraining the theoretical DE models with the SN Type Ia 292 data, after fixing the cosmological parameters in their viable range. Given below is the  $\chi^2$  statistic which has been used as a minimization technique for our data analysis,

$$\chi^2_{(SNeTypeIa)} = \sum \frac{(H(z) - H_{obs}(z))^2}{\sigma^2(z)} \quad (30)$$

where  $H_{obs}(z)$ ,  $\sigma(z)$  are obtained from the SNe Type Ia 292 data table and  $H(z)$  is the calculated value of the Hubble parameter obtained from our theoretical model. The probability distribution function is given as,

$$L = \int e^{-\frac{1}{2}\chi^2_{(SNeTypeIa)}} P(H_0) dH_0 \quad (31)$$

where the prior distribution function for  $H_0$  is  $P(H_0)$ . The best fit values of the model parameters ( $\omega_0, \omega_1$ ) obtained for different theoretical models by the  $\chi^2$  minimization technique is presented in table 5 along with their respective minimum  $\chi^2$  values. Contours, which are showing the numerical range of the parameters, are obtained for different confidence intervals and are given in the figs. 4a, 4b, 4c and 4d.

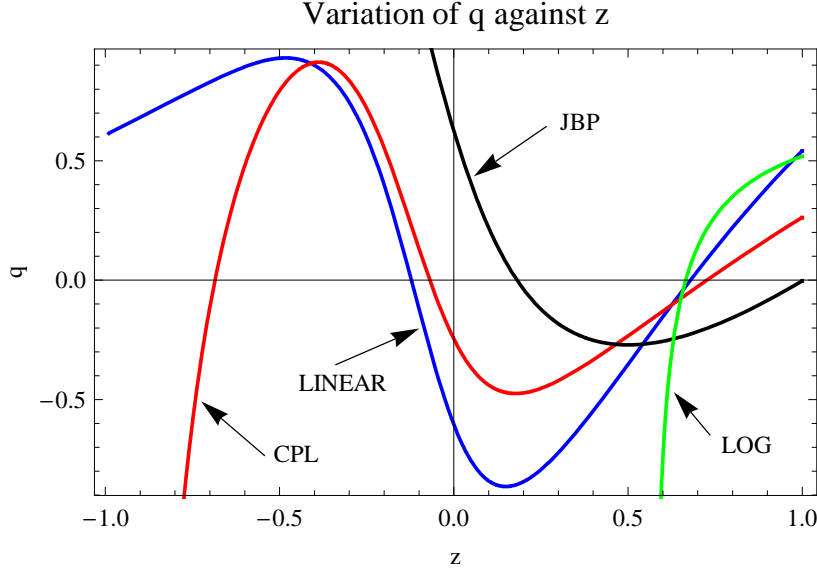


Fig.6

**Fig 6** shows the variation of deceleration parameter  $q$  vs redshift  $z$  for linear (Blue), CPL (Red), JBP (Black) and logarithmic (Green) parametrizations.

## 8 Discussions and conclusions

In this assignment, we have proposed the FRW universe filled with DM (perfect fluid with negligible pressure) along with dark energy in the background of Galileon gravity. For describing DE components, four parametrizations have been proposed for the variations of EOS parameter  $\omega(z)$ . They are Linear, CPL, JBP and Logarithmic parameterizations. We have presented the Hubble parameter  $H$  in terms of the observable parameters  $\Omega_{m0}$ ,  $\Omega_{de0}$ ,  $H_0$  with the redshift  $z$  and the other parameters like  $\omega_0$  and  $\omega_1$ . We have chosen the observed values of  $\Omega_{m0} = 0.28$ ,  $\Omega_{de0} = 0.72$  and  $H_0 = 72 \text{ Kms}^{-1} \text{ Mpc}^{-1}$ . From STERN data set (12 points), we have obtained the best fit values of the arbitrary parameters  $\omega_0$  and  $\omega_1$  (Table 2) by minimizing the  $\chi^2$  test and by fixing the other parameters. Similarly, the best fit values of  $\omega_0$  and  $\omega_1$  are presented in Table 3 and Table 4 for STERN+BAO and STERN+BAO+CMB respectively. In Table 5, the best fit values of the parameters are given using the Supernovae Type Ia 292 dataset. Likelihood contours have been drawn for different confidence levels (66%, 90%, 99%) constraining the parameters ( $\omega_0, \omega_1$ ). In the figs. 1a, 1b, 1c and 1d contours have been drawn for STERN data. In figs. 2a, 2b, 2c and 2d contours are drawn for STERN+BAO joint data analysis. STERN+BAO+CMB joint data have been used to generate the plots 3a, 3b, 3c and 3d. Contours for Supernovae Type Ia 292 data can be found in figs. 4a, 4b, 4c and 4d. Finally in figs. 5a and 5b, using the best fit values for our different theoretical parametrization models,  $\mu$  vs redshift ( $z$ ) curves are plotted and compared with Union compilation data and SNe Type Ia 292 data respectively.

Figs. 1a to 1d have been generated for Stern data. In fig. 1a, which is the plot for linear model, for 66% confidence interval  $\omega_0$  and  $\omega_1$  lies between  $-2.39$  to  $-1.51$  and  $0.78$  to  $1.16$  respectively. Similarly for 90% confidence limit, the ranges for  $\omega_0$  are  $-2.52$  to  $-1.58$  and those for  $\omega_1$  are  $0.74$  to  $1.18$ . For 99% confidence

limits the corresponding ranges for  $\omega_0$  are  $-2.67$  to  $-1.48$  and for  $\omega_1$  are  $0.68$  to  $1.22$ . From fig. 1b for CPL parametrization we see that for 66% confidence limits  $\omega_0$  lies between  $-2.12$  to  $-1.28$  and  $\omega_1$  lies between  $0.76$  to  $1.12$ . For 90% confidence limit  $\omega_0$  lies between  $-2.19$  to  $-1.21$  and  $\omega_1$  lies between  $0.72$  and  $1.14$ . Similarly for 99% limits the ranges are  $-2.34$  to  $-1.10$  for  $\omega_0$  and  $0.66$  to  $1.18$  for  $\omega_1$ . In fig. 1c, for JBP model, the corresponding ranges for  $\omega_0$  and  $\omega_1$  are  $-1.35$  to  $-0.65$  and  $-2.20$  to  $-1.45$  respectively, in 66% confidence limits. For 90% confidence limits the ranges are  $-1.50$  to  $-0.60$  for  $\omega_0$  and  $-2.22$  to  $-1.38$  for  $\omega_1$ . Finally for 99% confidence interval the values are  $-1.65$  to  $-0.55$  for  $\omega_0$  and  $-2.23$  to  $-1.27$  for  $\omega_1$ .

In fig. 2a for linear model (joint analysis with Stern+BAO), the ranges of parameters are  $-11.50$  to  $0.50$  for  $\omega_0$  and  $0.12$  to  $2.70$  for  $\omega_1$  in 66% confidence interval. For 90% confidence level,  $\omega_0$  varies from  $-12.30$  to  $0.61$  and  $\omega_1$  varies from  $-0.20$  to  $2.80$ . Finally for 99% confidence range,  $\omega_0$  varies from  $-13.20$  to  $0.90$  and  $\omega_1$  varies from  $-0.25$  to  $2.85$ . In fig. 2b, for the CPL model,  $\omega_0$  varies from  $-2.86$  to  $-1.89$  and  $\omega_1$  varies from  $1.47$  to  $2.25$  in 66% confidence interval. In 90%, confidence limits,  $\omega_0$  varies from  $-2.96$  to  $-1.80$  and  $\omega_1$  varies from  $1.42$  to  $2.70$ . For 99% confidence limits the variation is from  $-3.08$  to  $-1.68$  for  $\omega_0$  and  $1.30$  to  $2.11$  for  $\omega_1$ . Plot for JBP is generated in fig. 2c. We see that in 66% confidence interval,  $\omega_0$  varies from  $-1.31$  to  $-0.69$  and  $\omega_1$  varies from  $-3.61$  to  $-2.59$ . In 90% confidence limits,  $\omega_0$  varies from  $-1.39$  to  $-0.61$  and  $\omega_1$  varies from  $-3.72$  to  $-2.48$ . Similarly in 99% confidence limits,  $\omega_0$  and  $\omega_1$  varies respectively from  $-1.49$  to  $-0.56$  and  $-3.82$  to  $-2.30$ .

From figs. 3a to 3d, plots are generated for Stern+BAO+CMB joint data analysis. In fig. 3a, which is for linear model, the acceptable range for  $\omega_0$  is obtained as  $-3.59$  to  $-2.52$  and that for  $\omega_1$  is from  $1.30$  to  $1.73$  at 66% confidence level. Similarly at 90% confidence level the values of  $\omega_0$  vary from  $-3.76$  to  $-2.42$  and for  $\omega_1$  they vary from  $1.26$  to  $1.76$ . Finally for 99% confidence interval,  $\omega_0$  is from  $-3.96$  to  $-2.32$  and  $\omega_1$  is from  $1.17$  to  $1.81$ . In fig. 3b, for CPL model,  $\omega_0$  varies from  $-4.95$  to  $-3.05$  and  $\omega_1$  varies from  $0.61$  to  $0.81$  in 66% confidence level. In 90% confidence limits the ranges of  $\omega_0$  and  $\omega_1$  are respectively from  $-5.45$  to  $-2.95$  and  $0.55$  to  $0.85$ . Similarly for 99% limits, the acceptable range is from  $-6.05$  to  $-2.82$  for  $\omega_0$  and from  $0.49$  to  $0.89$  for  $\omega_1$ . In fig. 3c, the plot has been generated for JBP model. For 66% confidence interval,  $\omega_0$  takes the values from  $-4.8$  to  $-2.0$  and  $\omega_1$  takes the values from  $-1.4$  to  $-0.45$ . At 90% confidence interval, the acceptable ranges for  $\omega_0$  and  $\omega_1$  are  $-5.4$  to  $-1.9$  and  $-1.50$  to  $-0.43$  respectively. Finally at 99% confidence limits  $\omega_0$  varies from  $-6.5$  to  $-1.8$  and  $\omega_1$  varies from  $-1.7$  to  $-0.25$ .

Plots for SNe Type Ia 292 data are generated in figs. 4a to 4d for different parametrization models. In fig. 4a, for linear model, at 66% confidence level,  $\omega_0$  varies from  $-2.7142$  to  $-2.6980$  and  $\omega_1$  changes from  $0.5078$  to  $0.5116$ . At 90% confidence limits  $\omega_0$  ranges from  $-2.7159$  to  $-2.6964$  and  $\omega_1$  ranges from  $0.5074$  to  $0.5118$ . Finally at 99% confidence interval, the acceptable ranges are  $-2.7165$  to  $-2.6945$  for  $\omega_0$  and  $0.5070$  to  $0.5123$  for  $\omega_1$ . Fig. 4b is generated for the CPL model. Here at 66% confidence interval,  $\omega_0$  ranges from  $-2.6425$  to  $-2.6270$  and  $\omega_1$  ranges from  $0.5070$  to  $0.5105$ . At 90% confidence limits,  $-2.6442$  to  $-2.6247$  is the range for  $\omega_0$  and  $0.5066$  to  $0.5111$  is the range for  $\omega_1$ . Similarly at 99% confidence interval, the acceptable ranges vary from  $-2.6460$  to  $-2.6239$  for  $\omega_0$  and  $0.5062$  to  $0.5116$  for  $\omega_1$ . Plot for the JBP model has been obtained in fig. 4c. Here we see that,  $\omega_0$  and  $\omega_1$  respectively range from  $-2.3460$  to  $-2.3318$  and  $-1.0072$  to  $-0.9999$  for 66% confidence limit. At 90% confidence limits  $\omega_0$  attains values from  $-2.3475$  to  $-2.3302$ . Similarly the acceptable range for  $\omega_1$  is from  $-1.0078$  to  $-0.9990$ . Likewise, at 99% confidence limits the  $\omega_0$  lies in the range  $-2.3490$  to  $-2.3287$  and  $\omega_1$  lies in the range  $-1.0088$  to  $-0.9982$ .

For all the four cases the Logarithmic parametrization is studied in the figures 1d, 2d, 3d and 4d. In all the four figures it can be seen that the likelihood contours are parallel lines for all the three confidence levels. Unavailability of closed contours hinders our analysis considerably and due to this unbounded nature we are not able to put any finite bounds on both  $\omega_0$  and  $\omega_1$  from the present study and with the given choice of parameters. Looking at the figures, mathematically, one can obviously argue that the bound for the parameters are  $(-\infty, \infty)$ , but we do not think that it is physically acceptable. So, may be we have to devise some other methods to constrain the parameters for the logarithmic model, which we keep as an open issue for the time being.

On a general note, it is observed that for Linear and CPL model, with the increase in the value of  $\omega_0$ , the value of  $\omega_1$  decreases. But in case of JBP model, an exactly opposite nature is witnessed. Increase in  $\omega_0$  is accompanied by an increase in  $\omega_1$ . It must also be noted that for both the Linear and CPL model  $\omega_0$  lies in the negative range, whereas  $\omega_1$  takes positive values. For JBP model, the scenario is a bit different. Both  $\omega_0$  and  $\omega_1$  lies in the negative range. These results and the trends obtained for the involved parameters are quite different from the ones obtained by Biswas et al. in [68] using Loop quantum cosmology as background gravity. In [68], it was found that JBP model allows a wider range of values for the parameters compared to the linear and CPL models. Moreover with the addition of BAO peak analysis and CMB term the reduces the lower and

upper freedom of  $\omega_0$  and  $\omega_1$ . But in the present study no such trend is observed.

In the fig. 5a, distance modulus  $\mu(z)$  is plotted against redshift parameter  $z$  for all the four parametrization models and then compared with Union2 data Sample. The data sample is represented by a scatter diagram and the trajectories represent the  $\mu(z)$  vs  $z$  plots for various models. It is seen that barring the Logarithmic model, all the other models roughly fits the dataset. At lower redshifts ( $z < 0.3$ ) it is seen that the fit is not quite as good as that at higher redshifts. The best fit is obtained around  $z = 0.4$ . Moreover for the Logarithmic model, there is almost no fit with the data. In fig. 5b, the trajectories are compared with SNe Type Ia 292 data. Here also it is seen that the logarithmic model does not fit the dataset whereas the other three models gives satisfactory fit with the data. In this case, the fit is considerably improved at lower redshifts compared to the union 2 data sample. At higher redshifts the curve fitting is proper. The best fit is obtained around  $z = 0.5$ . Although the best fit point has shifted to a higher redshift in case of SNe Type Ia 292 dataset compared to the Union2 dataset, yet the SNe data must be preferred compared to its counterpart because it gives a better fit with the parametrization models at lower redshifts with the given choice of parameters. Alberto et al. in [69] used Bayesian analysis to predict that JBP parametrization is preferred to CPL. But in this assignment, we did not find any result, which will either support or criticize the prediction. Finally, it must be stated that from the present study, we find that the predicted theoretical Logarithmic model does not fit either of the observational data. Moreover, for the logarithmic model, no finite bounds for the parameters could be obtained.

In fig. 6, we have plotted the deceleration parameter  $q$  vs the redshift parameter  $z$ . Recently there have been quite a few works regarding cosmological deceleration acceleration transition [70, 71]. In these works it can be seen that the transition from deceleration to acceleration occurs at  $z = 0.74 \pm 0.05$ . We have obtained the expressions for the deceleration parameter for all the parametrization models using their best fit  $H(z) - z$  values of the parameters and then plotted them against redshift in fig. 6. From the figure it is seen that the transition from deceleration to acceleration regime occurs at  $z = 0.68$ ,  $z = 0.74$ ,  $z = 0.98$  and  $z = 0.67$  for the linear, CPL, JBP and logarithmic models respectively. So the result for the CPL model is in complete accordance with the works of Farooq et al. [70, 71]. Moreover the values for the linear and logarithmic models almost lie in the redshift spectrum of transition obtained in Farooq et al. Only in case of the JBP model the transition is early which contradicts the result obtained by Farooq et al. Finally it must be pointed out that since we have fixed the free parameters with particular values, we have lost the overall generality of the study upto a certain extent. Correspondingly the EoS contours obtained could have been much broader, if these particular choices could have been avoided. So the present study might have lost some of its numerical accuracy. Nevertheless its cosmological significance is unquestionable.

## Acknowledgements

The authors sincerely acknowledge the facilities provided by the Inter-University Centre for Astronomy and Astrophysics (IUCAA), pune, India where a part of the work was carried out. The Authors acknowledge the anonymous referee for enlightening comments that helped to improve the quality of the manuscript.

## References

- [1] S. J. Perlmutter et al. :- *Nature* **391** 51 (1998).
- [2] A. G. Riess et al. [Supernova Search Team Collaboration] :- *Astron. J.* **116** 1009 (1998).
- [3] A. G. Riess et al. :- *Astrophys. J.* **607** 665 (2004).
- [4] C. Bennet et al. :- *Phys. Rev. Lett.* **85** 2236 (2000).
- [5] D. N. Spergel et al. :- *Astrophys. J. Suppl. Ser.* **170** 377 (2007).
- [6] J. K. Adelman-McCarthy et al. :- *Astrophys. J. Suppl. Ser.* **175** 297 (2008).
- [7] T. Kobayashi, H. Tashiro, D. Suzuki :- *Phys. Rev. D.* **81** 063513 (2010)
- [8] D. J. Eisenstein et al. [SDSS Collaboration] :- *Astrophys. J.* **633** 560 (2005).
- [9] S. Briddle et al. :- *Science* **299** 1532 (2003).
- [10] D. N. Spergel et al. :- *Astrophys. J. Suppl.* **148**, 175 (2003).

- [11] P. J. E. Peebles, B. Ratra :- *Astrophys. J.* **325** L17 (1988).
- [12] R. R. Caldwell, R. Dave, P. J. Steinhardt :- *Phys. Rev. Lett.* **80** 1582 (1998).
- [13] C. Armendariz-Picon, V. F. Mukhanov, P. J. Steinhardt :- *Phys. Rev. Lett.* **85** 4438 (2000).
- [14] A. Sen :- *JHEP* **0207** 065 (2002).
- [15] R. R. Caldwell :- *Phys. Lett. B* **545** 23 (2002).
- [16] B. Feng, X. L. Wang, X. M. Zhang :- *Phys. Lett. B* **607** 35 (2005).
- [17] A. Y. Kamenshchik, U. Moschella, V. Pasquier :- *Phys. Lett. B* **511** 265 (2001).
- [18] U. Debnath, A. Banerjee, S. Chakraborty :- *Class. Quantum Grav.* **21** 5609 (2001).
- [19] A. Cohen, D. Kaplan, A. Nelson :- *Phys. Rev. Lett.* **82**, 4971 (1999).
- [20] V. Sahni, Y. Shtanov :- *JCAP* **0311** 014 (2003).
- [21] R. G. Cai :- *Phys. Lett. B* **657** 228 (2007).
- [22] H. Wei, R. G. Cai :- *Phys. Lett. B* **660** 113 (2008).
- [23] T. R. Choudhury, T. Padmanabhan :- *Astron. Astrophys.* **429** 807 (2007).
- [24] J. L. Tonry et al. :- *Astrophys. J.* **594** 1 (2003).
- [25] B. J. Barris et al. :- *Astrophys. J.* **602** 571 (2004).
- [26] J. Lu et al. :- *Phys. Lett. B* **662** 87 (2008).
- [27] L. Dao-Jun, L. Xin-Zhou :- *Chin. Phys. Lett.* **22** 1600 (2005).
- [28] G. R. Dvali, G. Gabadadze, M. Porrati :- *Phys. Lett. B* **484** 112 (2000).
- [29] A. De Felice, T. Tsujikawa :- *arXiv*: 1002.4928 [gr-qc].
- [30] S. Nojiri, S. D. Odintsov :- *arXiv*: 1011.0544 [gr-q].
- [31] T. Clifton, J. Barrow :- *Phys. Rev. D* **72** 103005 (2005).
- [32] K. K. Yerzhanov et al. :- *arXiv*:1006.3879v1 [gr-qc] (2010).
- [33] S. Nojiri, S. D. Odintsov :- *Phys. Lett. B* **631** 1 (2005).
- [34] I. Antoniadis, J. Rizos, K. Tamvakis :- *Nucl. Phys. B* **415** 497 (1994).
- [35] P. Horava :- *JHEP* **0903** 020 (2009).
- [36] C. Brans, H. Dicke :- *Phys. Rev.* **124** 925 (1961).
- [37] A. Nicolis, R. Rattazzi, E. Trincherini :- *Phys. Rev. D* **79** 064036(2009)
- [38] A. Melchiorri, L. Mersini, M. Trodden :- *Phys. Rev. D* **68** 043509(2003)
- [39] U. Seljak, A. Slosar, P. McDonald :- *JCAP* **0610** 014 (2006)
- [40] T. Padmanabhan, T. R. Chowdhury :- *Mon. Not. R. Astron. Soc.* **344** 823 (2003)
- [41] R. Amanullah et al. :- *Astrophys. J.* **716** 712 (2010).
- [42] C. Ranjit, P. Rudra, S. Kundu :- *Astrophys. Space Sci.* **347** 423(2013)
- [43] C. Ranjit, P. Rudra, U. Debnath :- *Can. J. Phys.* **92** 1667 (2014)
- [44] S. Chakraborty, U. Debnath, C. Ranjit :- *Eur. Phys. J. C.* **72** 2101(2012)
- [45] P. Thakur, S. Ghose, B. C. Paul:- *Mon. Not. R. Astron. Soc.* **397** 1935 (2009)
- [46] B. C. Paul, S. Ghose, P. Thakur :- *Mon. Not. R. Astron. Soc.* **413** 686 (2011)
- [47] F. P. Silva, K. Koyama :- *Phys. Rev. D* **80** 121301 (2009)
- [48] C. Deffayet, G. Esposito-Farese, A. Vikman :- *Phys. Rev. D* **79** 084003 (2009)
- [49] C. Deffayet, S. Deser, G. Esposito-Farese :- *Phys. Rev. D* **80** 064015 (2009)

- [50] N. Chow, J. Khoury :- *Phys. Rev. D* **80** 024037 (2009)
- [51] A. R. Cooray, D. Huterer :- *Astrophys. J.* **513** L95 (1999)
- [52] M. Chevallier, D. Polarski :- *Int. J. Mod. Phys. D.* **10** 213 (2001)
- [53] E. V. Linder :- *Phys. Rev. Lett.* **90** 091301 (2003)
- [54] P. Brax, J. Martin :- *Phys. Lett. B.* **468** 40 (1999)
- [55] H. K. Jassal, J. S. Bagla and T. Padmanabhan :- *Mon. Not. R. Astron. Soc.* **356** L11 (2005)
- [56] G. Efstathiou :- *Mon. Not. R. Astron. Soc.* **310** 842 (1999)
- [57] R. Silva, J. S. Alcaniz, J. A. S. Lima :- *Int. J. Mod. Phys. D.* **16**469 (2007)
- [58] D. Stern et al. :- *JCAP* **1002** 008 (2010).
- [59] J. R. Bond et al. :- *Mon. Not. Roy. Astron. Soc.* **291** L33 (1997)
- [60] G. Efstathiou, J. R. Bond :- *Mon. Not. R. Astro. Soc.* **304** 75 (1999)
- [61] S. Nessaeris, L. Perivolaropoulos :- *JCAP* **0701** 018 (2007).
- [62] E. Komatsu et al. :- *Astrophys. J. Suppl.* **192** 18 (2011).
- [63] S. J. Perlmutter et al. :- *Astrophys. J.* **517** 565 (1999).
- [64] A. G. Riess et al. :- *Astrophys. J.* **659** 98 (2007).
- [65] M. Kowalski et al. :- *Astrophys. J.* **686** 749 (2008).
- [66] P. Astier et. al. :- *Astron. Astrophys.* **447** 31 (2006)
- [67] C. Ranjit, U. Debnath :- *Astrophys. Space Sci.* **354** 2126 (2014), *arXiv:1409.7057 [phys-gen.ph]*
- [68] R. Biswas, U. Debnath :- *Eur. Phys. J. C.* **73** 2424 (2013)
- [69] J. Alberto Vazquez, M. Bridges, M.P. Hobson, A.N. Lasenby :- *arXiv:1205.0847 [astro-ph.CO]*
- [70] O. Farooq, B. Ratra :- *arXiv: 1301.5243 [astro-ph.CO]* (2013).
- [71] O. Farooq, S. Crandall, B. Ratra :- *arXiv: 1305.1957 [astro-ph.CO]* (2013).